

Importance of Cooling Speed on Rapid Synthesis of $\text{LiNi}_{0.5}\text{Mn}_{1.5}\text{O}_4$ by a Solution Combustion Synthesis Method

Guiyang Liu*, Yannan Li, Baosen Wang,

Lab of New Materials for Power Sources, College of Science, Honghe University, Mengzi, Yunnan, China, 661199

*E-mail: liuguiyang@tsinghua.org.cn

Received: 8 January 2015 / Accepted: 31 January 2015 / Published: 24 February 2015

Cooling speed is a significant factor for $\text{LiNi}_{0.5}\text{Mn}_{1.5}\text{O}_4$ synthesized by solution combustion synthesis method. In order to investigate the influence of cooling speed on $\text{LiNi}_{0.5}\text{Mn}_{1.5}\text{O}_4$ spinels, in this paper, $\text{LiNi}_{0.5}\text{Mn}_{1.5}\text{O}_4$ spinels have been synthesized by an improved solution combustion synthesis method at 800 °C for 10min with different cooling speed. X-ray diffraction (XRD), Fourier transform infrared spectroscopy (FTIR) and scanning electron microscope (SEM) have been used to investigate the phase composition and micro-morphologies of the products. Charge-discharge measurements, cyclic voltammetry (CV) and electrochemical impedance spectroscopy (EIS) have been used to study the electrochemical performance of the products. The results indicate that the fast cooled $\text{LiNi}_{0.5}\text{Mn}_{1.5}\text{O}_4$ (FC-LNMO) is single phase and possesses highly disordered phase structure and large amounts of Mn^{3+} ions. Contrastively, the slowly cooled product (SC-LNMO) is a combination of two phases, the main phase of $\text{LiNi}_{0.5}\text{Mn}_{1.5}\text{O}_4$ and the minor phase of $\text{Li}_x\text{Ni}_{1-x}\text{O}$ impurity. SC-LNMO has more ordered phase structure and possesses little amounts of Mn^{3+} ions. Although the reversible capacity of FC-LNMO is smaller than that of SC-LNMO, the cycle stability and rate capability of FC-LNMO are much better than these of SC-LNMO, due to the larger amounts of Mn^{3+} , lower polarization and smaller charge transfer resistance of FC-LNMO than these of SC-LNMO.

Keywords: Lithium ion batteries; solution combustion synthesis; $\text{LiNi}_{0.5}\text{Mn}_{1.5}\text{O}_4$ spinels; cooling speed

1. INTRODUCTION

Nowadays, lithium ion batteries can power most of today's portable electronic devices such as lap-top computers and mobile phones [1]. However, they still suffer limitations in some new applications such as hybrid electric vehicles (HEVs), electric vehicles (EVs) or power backup, which require both high energy and high power densities. In order to satisfy the high energy and high power

demands, good cathode materials for lithium ion batteries therefore should have high reversible storage for Li and rapid Li^+ and electron transport to obtain high capacity and high rate capability [2]. $\text{LiNi}_{0.5}\text{Mn}_{1.5}\text{O}_4$ spinels, which possess the advantages of high average discharge voltage (around 4.7 V vs. Li^+/Li couple), fast Li^+ diffusion within the three-dimensional spinel structure, low cost and environmental friendliness, have been regarded as one of the most promising candidates for high power and high energy cathode materials [3]. It has been reported that the final electrochemical performance of $\text{LiNi}_{0.5}\text{Mn}_{1.5}\text{O}_4$ can be affected significantly by the amount of Mn^{3+} ions, the structural ordering and the micro-morphology of $\text{LiNi}_{0.5}\text{Mn}_{1.5}\text{O}_4$ spinel, which strongly depend on the synthesis method and process [4]. Various synthesis methods including solid-state method [5], sol-gel method [6], Pechini method [7] or spray-drying method [8] producing $\text{LiNi}_{0.5}\text{Mn}_{1.5}\text{O}_4$ with different amount of Mn^{3+} ions, degree of structural ordering and micro-morphologies have been reported. Among them, solution combustion synthesis method is more attractive because it is simple, fast and efficient [9]. LiMn_2O_4 -based spinels synthesized by the solution combustion synthesis have been reported, which exhibit various electrochemical properties [10-12]. However, conventional solution combustion synthesis method generally uses metallic nitrates as metal source and carbonaceous compounds such as urea [13] or citric acid [14] as fuels. The combustion reaction between the nitrates and the fuel is violent, leading to a non-homogeneous precursor [15]. In order to obtain single phase $\text{LiNi}_{0.5}\text{Mn}_{1.5}\text{O}_4$, the precursor has to be annealed for a long time. Previously, we have developed an improved solution combustion synthesis method to synthesize LiMn_2O_4 -based spinels [16-18]. In this synthesis, metallic acetates were used to partly substitute the nitrate ones as raw materials, and the acetic radicals were the fuel themselves. The reaction rate could be decreased effectively, resulting in a more homogeneous precursor. Therefore, single phase spinels could be obtained at low temperature for short time [19].

In the solution combustion synthesis method, heat treatment is significant, because under different heat treatment, $\text{LiNi}_{0.5}\text{Mn}_{1.5}\text{O}_4$ would possess different amount of Mn^{3+} ions, structural ordering and micro-morphology [20]. We have noticed that the cooling speed after calcinations is very important for $\text{LiNi}_{0.5}\text{Mn}_{1.5}\text{O}_4$ synthesized by the improved solution combustion synthesis method. Faster cooling speed easily leads to larger amounts of Mn^{3+} and higher disordering of the phase structure in $\text{LiNi}_{0.5}\text{Mn}_{1.5}\text{O}_4$. In contrary, slower cooling speed generally results in less amount of Mn^{3+} and higher ordering of the phase structure. Therefore, it is worthwhile to understand the influence of the cooling speed on $\text{LiNi}_{0.5}\text{Mn}_{1.5}\text{O}_4$ synthesized by the solution combustion synthesis method.

In this paper, two $\text{LiNi}_{0.5}\text{Mn}_{1.5}\text{O}_4$ spinels have been synthesized by the improved solution combustion synthesis method under same experimental conditions except cooling speed. The one is cooled naturally in the furnace to room temperature after calcinations to get a slow cooling speed, and the other one is taken out immediately after calcinations and cooled down in air to get a fast cooling speed. The influences of cooling speed on the phase composition, structural ordering, micro morphology, and the amount of Mn^{3+} ions of the products have been investigated. Moreover, the influences of the cooling speed on the electrochemical performances including specific capacity, cycle stability and rate capability have been also studied.

2. EXPERIMENTAL

2.1 Preparation

About 20 g raw materials of LiNO_3 (AR, 99%), CH_3COOLi (AR, 99%), $\text{Mn}(\text{NO}_3)_2$ (AR, 99%), $(\text{CH}_3\text{COO})_2\text{Mn}$ (AR, 99%), $\text{Ni}(\text{NO}_3)_2$ (AR, 99%) and $(\text{CH}_3\text{COO})_2\text{Ni}$ (AR, 99%) with the mole ratio of 0.5:0.5:0.75:0.75:0.25:0.25 were firstly dissolved in 10 ml distilled water to obtain a solution. The solution was then put into a muffle furnace which presets at 800 °C and then ignited and combusted for 10 minutes. After that, for SC-LNMO, the furnace was stopped heating and then the sample was cooled in the furnace to room temperature naturally. For FC-LNMO, the sample was taken out from the furnace immediately after combustion and then cooled down to room temperature in air.

2.2 Characterization

The phase composition, structure ordering and micro morphology of the products were ascertained by XRD (D/max-rB, Cu-K α , within scattering angles of 10° and 70° in steps of 0.02°), FTIR (Perkin Elmer, with KBr pellets) and SEM (S4800, HITACHI).

2.3 Electrochemical performance test

The electrochemical characterizations were performed by using CR2032 coin-type cell. The test cell consisted of the $\text{LiNi}_{0.5}\text{Mn}_{1.5}\text{O}_4$ electrode as cathode electrode, lithium foil as anode electrode, a porous polypropylene film as a separator and 1 M LiPF_6 in EC/DMC (1:1 in volume) as an electrolyte. For $\text{LiNi}_{0.5}\text{Mn}_{1.5}\text{O}_4$ electrode fabrication, the prepared $\text{LiNi}_{0.5}\text{Mn}_{1.5}\text{O}_4$ powders were mixed with 10 wt % of carbon black and 10 wt% of polyvinylidene fluoride in N-methyl pyrrolidinone until slurry was obtained. Then, the blended slurries were pasted onto an aluminum current collector, and the electrode was dried at 120°C for 12 h in vacuum. The cells were assembled in an argon-filled glove box and cycled at room temperature. The electrochemical performances of the products were evaluated upon cycling in the 3.5 - 5.0V versus Li/Li^+ electrode at different C rate. Here 1C=150mA/g. Cyclic voltammograms (CV) were carried out by an electrochemical workstation (AUT302N, Metrohm, Switzerland) with a scan rate of 0.1 - 0.5 mV/s between 3.5-5.0 V. Electrochemical impedance spectroscopy (EIS) were collected at 100% state of charge at 5V with an AC amplitude of 5 mV in the frequency range of 10 kHz to 0.1 Hz, and Li foil was used as both counter and reference electrodes.

3. RESULTS AND DISCUSSION

3.1 Phase structure and micro-morphologies

Phase composition of the products can be determined by XRD. The XRD patterns of FC-LNMO and SC-LNMO are shown in Fig.1. As shown in Fig. 1a, all peaks of the product correspond to

$\text{LiNi}_{0.5}\text{Mn}_{1.5}\text{O}_4$ (JCPDS 80-2162, $a=0.817\text{nm}$) and no evident other peaks could be found, suggesting that FC-LNMO is a single phase $\text{LiNi}_{0.5}\text{Mn}_{1.5}\text{O}_4$ spinel. For SC-LNMO (as seen in Fig. 1b), although the strong peaks correspond to $\text{LiNi}_{0.5}\text{Mn}_{1.5}\text{O}_4$, but there are some weak peaks in the pattern, which are attributed to $\text{Li}_x\text{Ni}_{1-x}\text{O}$. Moreover, it also can be seen from Fig.1 that the relative intensities of the peaks of SC-LNMO (Fig.1b) are stronger than there of FC-LNMO (Fig.1a), and the calculated average grain size from the XRD data of SC-LNMO and FC-LNMO are 391 nm and 112 nm, respectively, indicating that the crystallinity of SC-LNMO is higher than that of FC-LNMO.

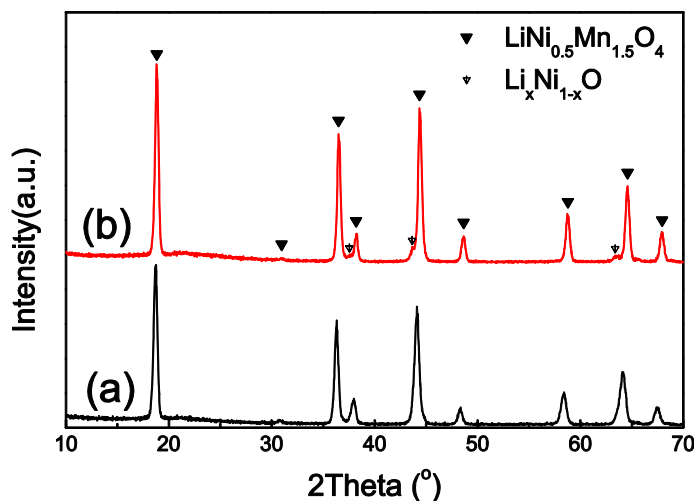


Figure 1. XRD patterns of (a) FC-LNMO and (b) SC-LNMO.

There are two types of $\text{LiNi}_{0.5}\text{Mn}_{1.5}\text{O}_4$ spinel with different space groups, disordered $Fd-3m$ or ordered $P4_332$ [21]. It has been reported that most of the reported high-voltage $\text{LiNi}_{0.5}\text{Mn}_{1.5}\text{O}_4$ spinels are non-stoichiometric, disordered, and oxygen deficient due to the high-temperature calcination [22]. For the non-stoichiometric $\text{LiNi}_{0.5}\text{Mn}_{1.5}\text{O}_{4-x}$ spinel, accompanied by the loss of oxygen, part of the inactive Mn^{4+} ions are reduced to Mn^{3+} due to the charge neutrality. Because Mn^{3+} ion has a larger ionic radius than that of Mn^{4+} ion, the lattice parameters of the non-stoichiometric $\text{LiNi}_{0.5}\text{Mn}_{1.5}\text{O}_{4-x}$ spinel generally increase with increasing amounts of Mn^{3+} ions in the lattice [23]. The calculated lattice parameter of FC-LNMO is 0.8217nm, much larger than that of the standard lattice parameter of 0.817 nm. It suggests that the FC-LNMO is a non-stoichiometric $\text{LiNi}_{0.5}\text{Mn}_{1.5}\text{O}_{4-x}$ with moderate amounts of Mn^{3+} and oxygen deficient in the product due to the fast cooling speed. In contrary, the calculated lattice parameter of SC-LNMO is 0.8166 nm, similar as the standard one, suggesting that the SC-LNMO is a more stoichiometric $\text{LiNi}_{0.5}\text{Mn}_{1.5}\text{O}_4$ with little amounts of Mn^{3+} ions and oxygen deficient.

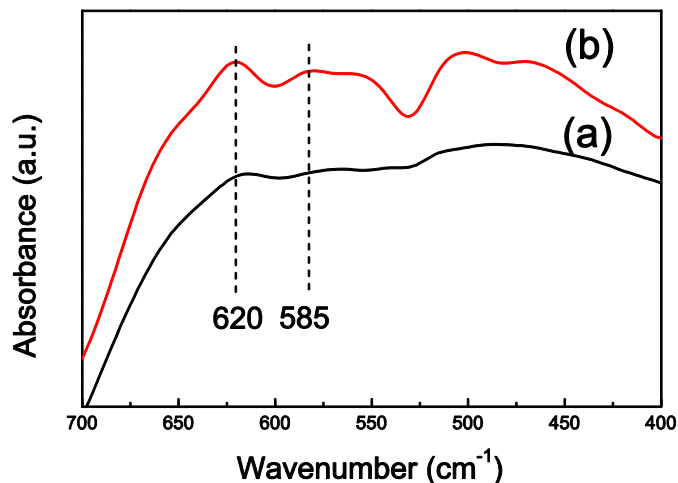


Figure 2. FTIR spectra patterns of (a) FC-LNMO and (b) SC-LNMO.

However, the structural ordering of $\text{LiNi}_{0.5}\text{Mn}_{1.5}\text{O}_4$ is hardly to be distinguished by normal X-ray diffraction directly because the scattering factors of Ni and Mn are similar [24]. FTIR spectroscopy has been proved to be an effective technique in qualitatively resolving the cation ordering [25]. Characteristic infrared vibration bands of the M–O bonds of the sample between 700 cm^{-1} and 400 cm^{-1} were used to determine the structural ordering in $\text{LiNi}_{0.5}\text{Mn}_{1.5}\text{O}_4$. With increasing degree of lattice ordering, the intensity of Ni–O band at about 588 cm^{-1} increases while the intensity of Mn–O band at 620 cm^{-1} decreases [26]. As shown in Fig.2a, there is no evident peak appeared at about 588 cm^{-1} , suggesting that FC-LNMO is a highly disordered $\text{LiNi}_{0.5}\text{Mn}_{1.5}\text{O}_4$. From Fig.2b, there is an obvious peak appeared at 586 cm^{-1} , but the band intensity at 586 cm^{-1} is lower than that at 620 cm^{-1} . It suggests that SC-LNMO is also a disordered $\text{LiNi}_{0.5}\text{Mn}_{1.5}\text{O}_4$, but its structural ordering is higher than that of FC-LNMO [27].

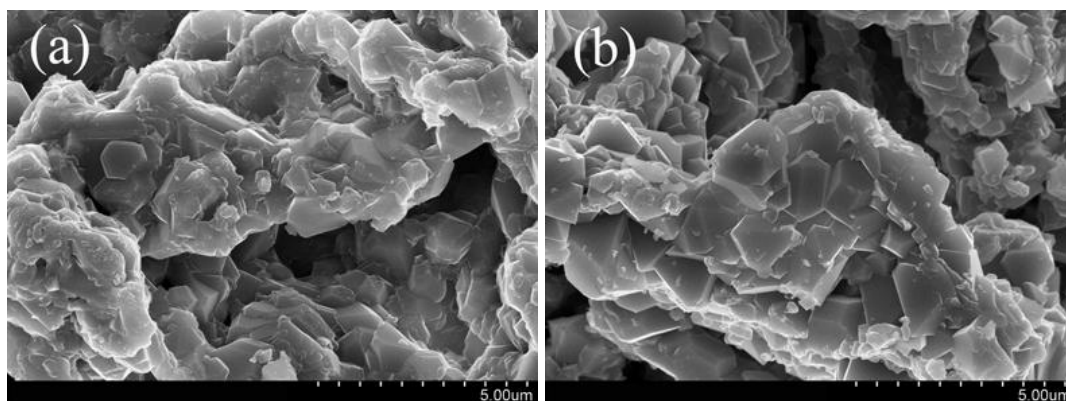


Figure 3. SEM images of (a) FC-LNMO and (b) SC-LNMO.

Fig.3 shows the SEM images of the products. It can be found that the grain size of SC-LNMO (as shown in Fig.3b) is larger than that of FC-LNMO (as shown in Fig.3a), and the surface facets of

SC-LNMO are clearer than these of FC-LNMO. These indicate that the grains of SC-LNMO are more developed and the crystallinity of SC-LNMO is higher than these of FC-LNMO, which are in agreement with the XRD results.

3.2 Electrochemical performance

The electrochemical charge/discharge studies of the products were performed in a galvanostatic mode between 3.5 and 5.0 V at 0.2C charge/discharge rate. The initial voltage profiles of the products are shown in Fig.4a. The charge/discharge curves show two main voltage plateaus in 4.7 V and 4.0 V regions, respectively. The plateau at 4.7V has been ascribed to the two-steps ($\text{Ni}^{4+}/\text{Ni}^{3+}$, $\text{Ni}^{3+}/\text{Ni}^{2+}$) redox reactions, and the plateau at 4V reflects the redox reaction between the Mn^{3+} and Mn^{4+} couple [28]. It can be seen from Fig.4a that the charge/discharge curves of FC-LNMO show flat voltage plateaus in the 4.0 V regions with similar length as the plateaus in 4.7V regions, suggesting that the redox reaction between the Mn^{3+} and Mn^{4+} couples of FC-LNMO is obvious and the amount of Mn^{3+} in FC-LNMO is considerable.

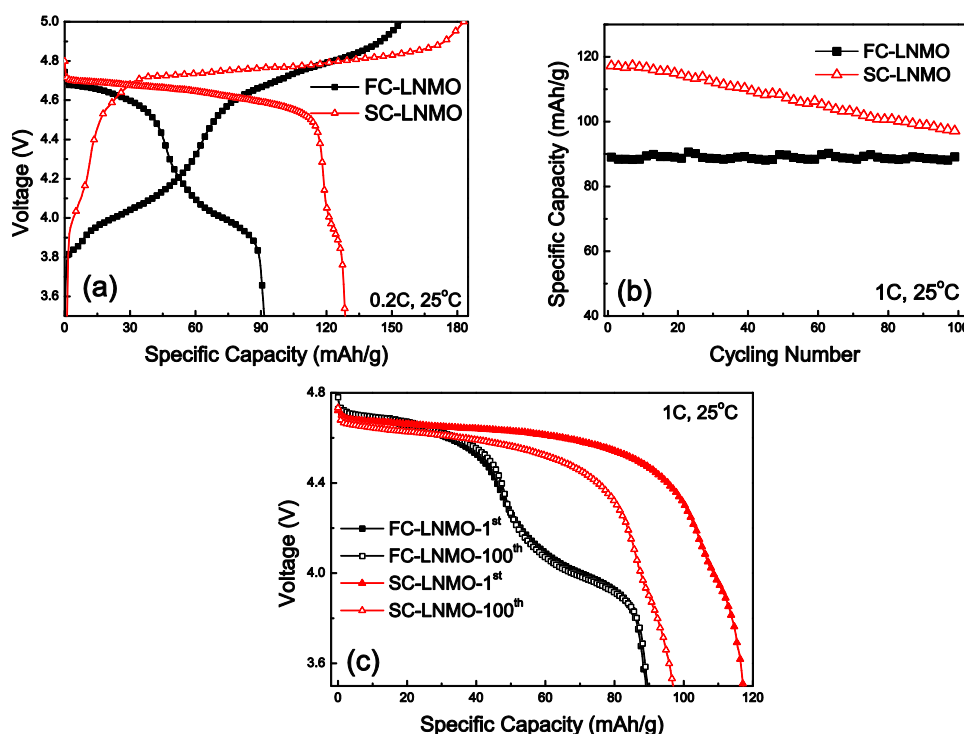


Figure 4. (a) Initial charge/discharge curves of the products versus metal Li. The test was performed in a constant current and constant voltage mode. The cell was charged with a constant current of 0.2C (about 30mA/g) to 5.0 V, held at 5.0 V for 10min and then discharged at 0.2C to 3.5 V. (b) Cycling performance and (d) the comparison of the 1st and the 100th discharge curves of the products at 1C rate. The test was performed at 1C discharge rate and 0.5C charge rate within the voltage range of 3.5-5.0V.

In contrary, the voltage plateau in the 4.0V region of SC-LNMO is not obvious, indicating that the amount of Mn^{3+} in SC-LNMO is little [23]. The percentages of capacity contribution from the 4.0 V plateau of the samples can be calculated from the capacity between 3.80 and 4.25 V divided by the total discharge capacity and can be qualitatively used to evaluate the relative concentration of Mn^{3+} ions in the spinels [23]. About 41.2% and 6.1% of the total capacities from 4.0V plateaus of FC-LNMO and SC-LNMO are obtained, respectively. It confirms that FC-LNMO has large amounts of Mn^{3+} ions and SC-LNMO has little amounts of Mn^{3+} ions in the lattice, which is consistent with the XRD and FTIR results.

The initial discharge capacity of SC-LNMO is 128.6 mAh/g, which is much higher than 91.5 mAh/g of FC-LNMO. Because there are large amounts of Mn^{3+} ions in FC-LNMO, for charge neutrality, it will induce the loss of oxygen, or induce Ni^{2+} to be oxidized to Ni^{3+} or Ni^{4+} . The capacity contribution from 4.7V plateau could be approximately calculated from the capacity >4.4V, which is attributed to Ni^{2+} ions in the spinels. The calculated capacities from 4.7V of FC-LNMO and SC-LNMO are 44 and 116 mAh/g, respectively. The results clearly show that the capacity from 4.7V plateau of FC-LNMO is much smaller than that of SC-LNMO. It suggests that a part of Ni^{2+} ions in FC-LNMO are oxidized, resulting in smaller reversible capacity than that of SC-LNMO.

Cycling performances of the products at 1C at 25 °C are shown in Fig.4b. The capacity retentions after 100 cycles of FC-LNMO and SC-LNMO are 99.6% and 82.8%, respectively. After 100 cycles, the plateau voltage in the discharge curve of FC-LNMO changes much less than that of SC-LNMO (as seen in Fig.4c), suggesting that the cycling stability of FC-LNMO is much higher than that of SC-LNMO. Park [29] and Shin [30] reported that disordered $LiNi_{0.5}Mn_{1.5}O_4$ spinels with appropriate amounts of Mn^{3+} ions have better electrochemical performances than these of the ordered $LiNi_{0.5}Mn_{1.5}O_4$ spinels without Mn^{3+} ions. FC-LNMO in this paper possessing a more disordered phase structure and larger amounts of Mn^{3+} ions therefore has better cycling performance.

Rate capability is important for lithium ion batteries. The rate capabilities of the products are shown in Fig.5. Both FC-LNMO and SC-LNMO show excellent capacity retentions with increasing rate (as seen in Fig.5a). Although SC-LNMO exhibits larger reversible capacities at different rate than these of FC-LNMO, FC-LNMO exhibits better capacity retentions than these of SC-LNMO. Here we chose the initial discharge capacity of the electrode at 0.2C as 100% for comparison. It is found that FC-LNMO remains 98.1%, 97.8%, 96.6%, 92.6% and 81.9% of the capacity (0.2C) at discharge rate of 0.5, 1, 2, 5 and 10C, respectively. For SC-LNMO, the capacity remains 98.4%, 95.2%, 91.0%, 83.2% and 72.8% at 0.5C, 1C, 2C, 5C and 10C, respectively.

From Fig.5b and Fig.5c, it can be found that the polarizations of the two products from 0.2C to 2C are small, suggesting that at low rate, both FC-LNMO and SC-LNMO exhibit good rate capabilities. However, at above 5C, the operation voltages of FC-LNMO are higher than these of SC-LNMO. It suggests that the polarization of FC-LNMO is larger than that of SC-LNMO with increasing rate. It has been reported that the existence of Mn^{3+} ions [23, 31] and the increase of oxygen non-stoichiometries in $LiNi_{0.5}Mn_{1.5}O_4$ [25] can improve the rate performance. FC-LNMO possessing much larger amounts of Mn^{3+} ions than these of SC-LNMO therefore exhibits much better rate capability than that of SC-LNMO. Fig.5d shows the cycling performances of the two products at 10C. After 100 cycles at 10C rate, the capacity retention of FC-LNMO is near 100%. In contrast, the capacity

retention of SC-LNMO is only 90.1%. FC-LNMO exhibits excellent cycling abilities at high rate. Nevertheless, it is noticeable that although the rate capability of SC-LNMO is inferior to that of FC-LNMO, compared with some previously reported pristine $\text{LiNi}_{0.5}\text{Mn}_{1.5}\text{O}_4$ [21, 32], the rate capability of SC-LNMO is better.

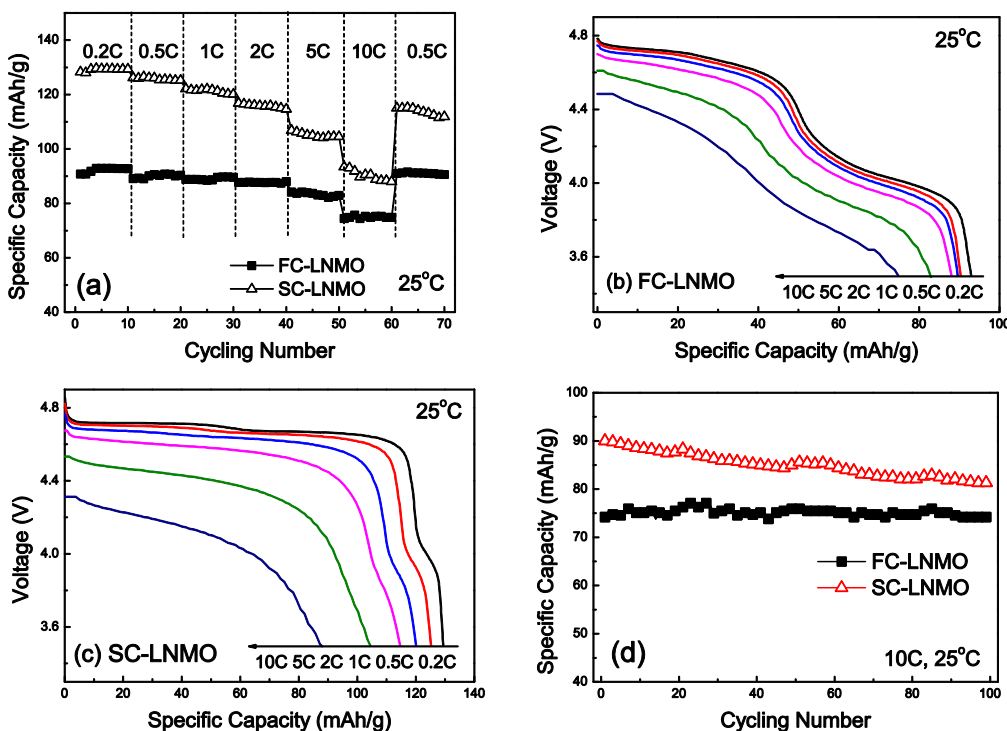


Figure 5. (a) Discharge capacity vs rates of the products. (b) Charge/discharge curves of FC-LNMO. (c) Charge/discharge curves of SC-LNMO. (d) Cycling performance of the products at 10C rate. A slow charge rate of 0.5C was used to effectively evaluate the ability of the host spinel structures to accommodate Li^+ ions when discharge rate is $\geq 0.5\text{C}$.

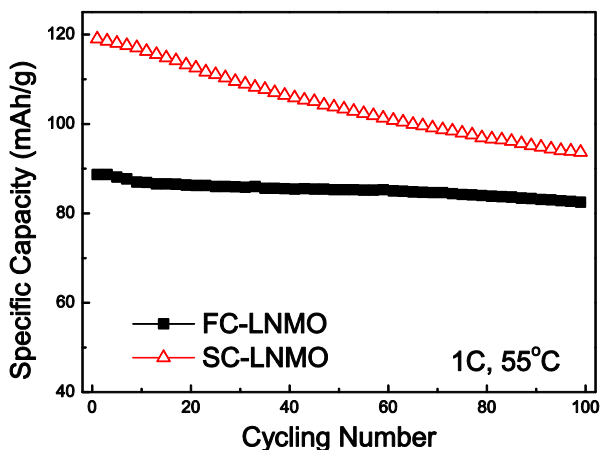


Figure 6. Cycling performance of the products at 1C rate at 55°C. The test was performed at 1C discharge rate and 0.5C charge rate within the voltage range of 3.5-5.0V.

The main drawback of the $\text{LiNi}_{0.5}\text{Mn}_{1.5}\text{O}_4$ -based cathodes is the severe capacity loss at elevated temperature ($55\text{ }^\circ\text{C}$) [33]. Fig. 6 shows the cycling performances of the products in the voltage range of 3.5-5.0V at 1C rate at $55\text{ }^\circ\text{C}$. After 100 cycles, the capacity retention of FC-LNMO is 93.0%, meanwhile the capacity retention of SC-LNMO is only 78.4%. FC-LNMO shows much better cycling stability at the elevated temperature than that of SC-LNMO. Compared with the reported pristine $\text{LiNi}_{0.5}\text{Mn}_{1.5}\text{O}_4$ [34], the capacity retention of FC-LNMO is also better. It confirms that Mn^{3+} ions in $\text{LiNi}_{0.5}\text{Mn}_{1.5}\text{O}_4$ are important for improving the electrochemical performance of $\text{LiNi}_{0.5}\text{Mn}_{1.5}\text{O}_4$.

To gain further insight into the electrochemical characteristics, a series of voltammetry measurements of the products were performed. Fig.7 shows the cyclic voltammogram (CV) of the products recorded at 0.1mV/s to 0.5mV/s scan rates, respectively. There are two regions in the CVs, 4.0V region and 4.7V region.

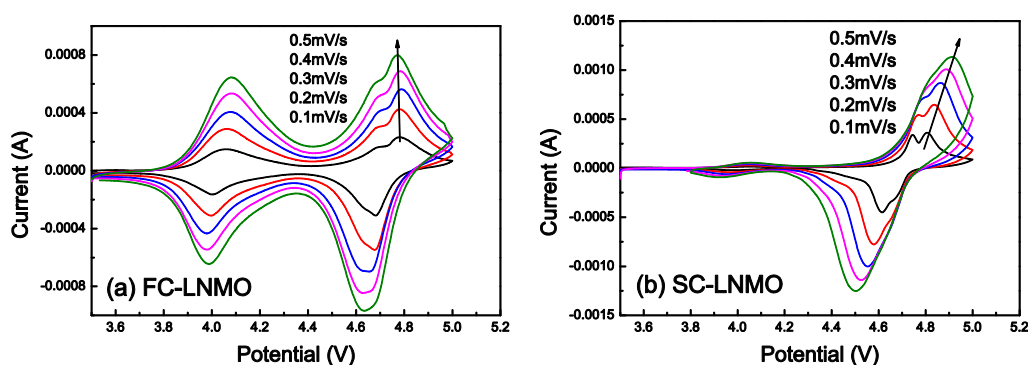


Figure 7. Cyclic voltammograms (CV) of (a) FC-LNMO and (b) SC-LNMO at different scan rate.

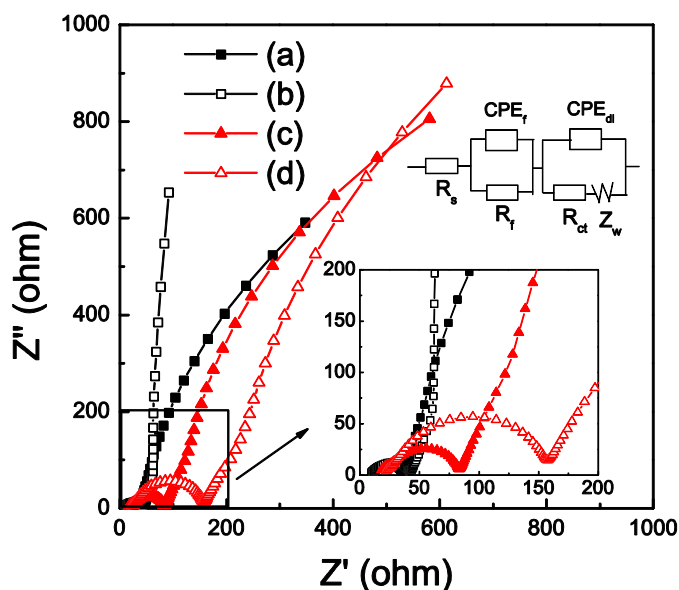


Figure 8. EIS spectra of (a) FC-LNMO after 5 cycles, (b) FC-LNMO after 100 cycles, (c) SC-LNMO after 5 cycles and (d) SC-LNMO after 100 cycles.

From Fig.7a it can be found that the peak intensities of the two redox pair in 4.0V region of FC-LNMO are very strong, suggesting that there are large amounts of Mn^{3+} ions in FC-LNMO. However, for SC-LNMO (as seen in Fig.7b), the peak intensities of the two redox pair in 4.0V region are weak, suggesting there are little amounts of Mn^{3+} in SC-LNMO. The results are consistent with the results of charge/discharge curves. Moreover, it can be seen from Fig.7 that with the increase of scan rate from 0.1 to 0.5 mV/s, the changes of the voltage gaps between each redox couple of FC-LNMO are little. In contrary, the changes of SC-LNMO are much larger than these of FC-LNMO. It suggests that the polarization of FC-LNMO is much smaller than that of SC-LNMO, which is in accord with the rate test results.

Fig.8 shows the electrochemical impedance spectra (EIS) of the batteries with different samples as electrodes after 5th and 100th cycles. The plot includes the real component of the impedance on the horizontal axis (Z'), and the imaginary component of the impedance on the vertical axis (Z''). The EIS spectrums are combination of the depressed semicircle at high-to-middle frequency region and an inclined line in the low frequency region. The intercept at the Z' axis corresponds to the ohmic resistance (R_s), the semicircle is related closely to the lithium-ion migration resistance (R_f) through the multilayer surface films and the charge transfer resistance (R_{ct}) in high-to-middle frequency range [35], and the inclined line in the low frequency region is the Warburg impedance of solid phase diffusion (σ_w), which is related to the lithium-ion diffusion in the spinel particles [36]. Apparently, it can be seen from Fig.8 that the R_{ct} of FC-LNMO (Fig.8a) is much smaller than that of SC-LNMO (Fig.8c). Moreover, after 100 cycles, the R_{ct} of FC-LNMO (Fig.8b) changes little, meanwhile the R_{ct} of SC-LNMO (Fig.8d) is increased obviously, suggesting that the conductivity of FC-LNMO changes little after cycles. It has been reported that lower R_{ct} value of $LiNi_{0.5}Mn_{1.5}O_4$ means a lower electrochemical polarization, which can lead to higher rate cycling performance [21], and higher R_{ct} signifies the more capacity loss at the high charge/discharge rate [37]. FC-LNMO possessing lower R_{ct} before and after cycles than these of SC-LNMO therefore exhibits better rate capability than that of SC-LNMO, which is in good agreement with the C-rate capacity data.

4. CONCLUSION

$LiNi_{0.5}Mn_{1.5}O_4$ spinels have been synthesized by an improved solution combustion synthesis method at 800 °C for 10min with different cooling speed. The fast cooled $LiNi_{0.5}Mn_{1.5}O_4$ has highly disordered phase structure and large amounts of Mn^{3+} ions in the lattice. The slowly cooled $LiNi_{0.5}Mn_{1.5}O_4$ has more ordered phase structure and little amounts of Mn^{3+} ions. Although the reversible capacity of the fast cooled $LiNi_{0.5}Mn_{1.5}O_4$ is smaller than that of the slowly cooled $LiNi_{0.5}Mn_{1.5}O_4$, the cycle stability and rate capability of the fast cooled $LiNi_{0.5}Mn_{1.5}O_4$ are much better than that of the slowly cooled $LiNi_{0.5}Mn_{1.5}O_4$, due to its larger amounts of Mn^{3+} ions, lower polarization and smaller charge transfer resistance.

ACKNOWLEDGEMENT

The present work was supported by the National Natural Science Foundation of China (No. 51362012), Natural Science Foundation of Yunnan Province (2012FB173).

Reference

1. H. Li, Z. Wang, L. Chen, X. Huang, *Adv. Mater.*, 21(2009) 4593.
2. K. Kang, Y.S. Meng, J. Bre'ger, C.P. Grey, G. Ceder, *Science*, 311 (2006) 977.
3. B.L. Ellis, K.T. Lee, L.F. Nazar, *Chem. Mater.*, 22 (2010) 691.
4. Y. Sun, Y. Yang, H. Zhan, H. Shao, Y. Zhou, *J. Power Sources*, 195 (2010) 4322.
5. C. Peng, H. Bai, M. Xiang, C. Su, G. Liu, J. Guo, *Int. J. Electrochem. Sci.*, 9 (2014) 1791.
6. B. Hwang, Y. Wu, M. Venkateswarlu, M. Cheng, R. Santhanam, *J. Power Sources*, 193 (2009) 828.
7. M. Kunduraci, G.G. Amatucci, *Electrochim. Acta*, 53 (2008) 4193.
8. D.C. Li, A. Ito, K. Kobayakawa, H. Noguchi, Y. Sato, *Electrochim. Acta*, 52 (2007) 1919.
9. M.G. Lazarraga, L. Pascual, H. Gadjev, D. Kovacheva, K. Petrov, J.M. Amarilla, R.M. Rojas, M.A. Martin-Luengoa, J.M. Rojo, *J. Mater. Chem.*, 14 (2004) 1640.
10. M.Y. Mo, C.C. Ye, K. Lai, Z. Huang, L. Zhu, G. Ma, H. Chen, K.S. Hui, *Appl. Surf. Sci.*, 276 (2013) 635.
11. J.M. Amarilla, K. Petrov, F. Picó, G. Avdeev, J.M. Rojo, R.M. Rojas, *J. Power Sources*, 191 (2009) 91.
12. M.A. Kebede, N. Kunjuzwa, C.J. Jafta, M.K. Mathe, K.I. Ozoemena, *Electrochim. Acta*, 128 (2014) 172.
13. S. Chitra, P. Kalyani, T. Mohan, *J. Electroceram.*, 3 (1999) 433.
14. W. Wen, J. Wu, J. Tu, *J. Alloy. Compd.*, 513 (2012) 592.
15. G. Fey, Y. Cho, T. Kumar, *Mater. Chem. Phys.*, 99 (2006) 451.
16. M. Xiang, C. Su, L. Feng, M. Yuan, J. Guo, *Electrochim. Acta*, 125 (2014) 524.
17. G. Liu, X. Kong, Q. Wang, H. Sun, B. Wang, Z. Yi, *Ceram. Int.*, 40 (2014) 6447.
18. G. Liu, K. Xin, L. Zhang, B. Wang, Y. He, *Mater. Sci.-Poland*, 31(2013) 386.
19. G. Liu, X. Kong, B. Wang, *J. Electrochem Soc.*, 161 (2014) A742.
20. J.W. Wen, D.W. Zhang, Y. Zang, X. Sun, B. Chen, C.X. Ding, Y. Yu, C.H. Chen, *Electrochim. Acta*, 133 (2014) 515.
21. T. Yi, Y. Xie, Y. Zhu, R. Zhu, M. Ye, *J. Power Sources*, 211 (2012) 59.
22. M.I. Zaki, M.A. Hasan, L. Pasupulety, K. Kumari, *Thermochim. Acta*, 2 (1997) 171.
23. J. Xiao, X. Chen, P.V. Sushko, M.L. Sushko, L. Kovarik, J. Feng, Z. Deng, J. Zheng, G.L. Graff, Z. Nie, D. Choi, J. Liu, J. Zhang, M. Whittingham, *Adv. Mater.* 24 (2012) 2109.
24. H. Fang, L. Li, G. A. Li, *J. Power Sources*, 167 (2007) 223.
25. Y. Jin, C. Lin, J. Duh, *Electrochim. Acta*, 69 (2012) 45.
26. L. Wang, H. Li, X. Huang, E. Baudrin, *Solid State Ionics*, 193 (2011) 32.
27. E. Lee, K. Nam, E. Hu, A. Manthiram, *Chem. Mater.*, 24 (2012) 3610.
28. S. Patoux, L. Daniel, C. Bourbon, H. Lignier, C. Pagano, F.L. Cras, S. Jouanneau, S. Martinet, *J. Power Sources*, 189 (2009) 344.
29. J. Park, K.C. Roh, J.W. Lee, K. Song, Y. Kim, Y.M. Kang, *J. Power Sources*, 230 (2013) 138.
30. D.W. Shin, C.A. Bridges, A. Huq, M.P. Paranthaman, A. Manthiram, *Chem. Mater.*, 24 (2012) 3720.
31. U. Lafont, C. Locati, W.J.H. Borghols, A. Łasin'ska, J. Dygas, A.V. Chadwick, E.M. Kelder, *J. Power Sources*, 189 (2009) 179.
32. D.W. Shin, A. Manthiram, Surface-segregated, *Electrochem. Commun.*, 13 (2011) 1213.
33. M. Akhalouch, R.M. Rojas, J.M. Rojo, I. Saadoune, J.M. Amarilla, *Electrochim. Acta*, 54 (2009) 7542.
34. J. Chae, S.B. Yoon, W.S. Yoon, Y.M. Kang, S.M. Park, J.W. Lee, *J. Alloys Compd.*, 601 (2014) 217.
35. J. Liu, A. Manthiram, *Chem. Mater.*, 21 (2009) 1695.
36. K.A. Striebel, E. Sakai, E.J. Cairns, *J. Electrochem Soc.*, 149 (2002) A61.

37. Y.Z. Wang, X. Shao, H. Xu, M. Xie, S. Deng, H. Wang, J. Liu, H. Yan, *J. Power Sources*, 226 (2013) 140

© 2015 The Authors. Published by ESG (www.electrochemsci.org). This article is an open access article distributed under the terms and conditions of the Creative Commons Attribution license (<http://creativecommons.org/licenses/by/4.0/>).